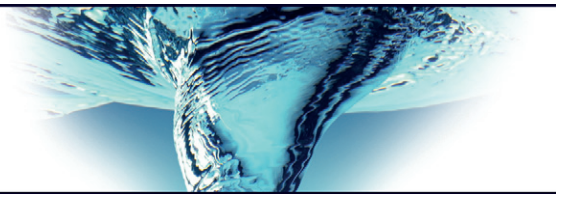
J. Fluid Mech. (2015), *vol.* 781, R6, doi:10.1017/jfm.2015.514



JFM RAPIDS
journals.cambridge.org/rapids

Self-sustained states at Kolmogorov microscale

Kengo Deguchi†

Department of Mathematics, Imperial College London, South Kensington Campus, London SW7 2AZ, UK

(Received 27 May 2015; revised 30 July 2015; accepted 3 September 2015; first published online 28 September 2015)

It is shown theoretically how the scaling of coherent structures in shear flows changes their asymptotic development at large Reynolds number. Based on the theory a family of nonlinear self-sustained states at Kolmogorov microscale is numerically identified on the laminar–turbulent boundary of shear flows. Theoretically and numerically the states connect to known asymptotic states existing at larger scale. The asymptotically very small amplitude of the new states may explain why strongly sheared, linearly stable laminar flows can cause a turbulent transition by small disturbances. The numerically obtained Kolmogorov-scale solutions can be used to describe the theoretically minimal self-sustained structures appearing in various shear flows.

Key words: mathematical foundations, nonlinear instability, transition to turbulence

1. Introduction

The inaccurate agreement of the linear stability theory with shear-flow experiments is widely known. The linear stability boundary in the parameter space is only realized for extremely small disturbances; see Nishioka, Iida & Ichikawa (1975) for example. Furthermore, for some flows, such as plane Couette or pipe flows, there is no linear instability at all, although in reality these flows experience a laminar–turbulent transition by small perturbations. This mismatch of the theory and observations was pointed out by Sommerfeld (1908).

Obviously, the key to the resolution of the mismatch is the nonlinearity of the disturbances. Therefore, nonlinear solutions of Navier–Stokes equations have attracted much attention; see Nagata (1990), Clever & Busse (1997) and Waleffe (2003). In the shear-flow transition community, the nonlinear solutions are called 'exact coherent structures' due to their resemblance to the streaky coherent structures in shear flows. Recently, further theoretical progress has been made by Hall & Sherwin (2010) using the self-consistent formal asymptotic theory for large Reynolds number, originally

† Email address for correspondence: k.deguchi@imperial.ac.uk

© Cambridge University Press 2015

https://doi.org/10.1017/jfm.2015.514 Published online by Cambridge University Press

developed earlier (Hall & Smith 1991). The theory, called vortex–wave interaction (VWI), explains that the streamwise vortex seen in the solutions is sustained by a wave excited by an inviscid instability of the streak. That wave is governed by Rayleigh equation in the limit of large Reynolds number, and thus sometimes called a Rayleigh wave. In the literature regarding exact coherent structures at finite Reynolds numbers, a simpler and more 'physical' representation of the interaction compared with the more complicated and rigorous VWI approach is known as a 'self-sustaining process'; see Waleffe (1997). Importantly, the exact coherent structures of VWI type sit at the edge of laminar–turbulent attractors, as shown by Itano & Toh (2001) and Wang, Gibson & Waleffe (2007).

Although the studies mentioned above have significantly enhanced our understanding of the shear-flow transition, another puzzle has emerged. On the one hand, according to the VWI theory/self-sustaining process, the streaky field must be modulated by an amount $O(1)$ to produce a wave-like instability when the basic flow is inviscidly stable, but on the other hand Duguet *et al.* (2013) showed numerically that the optimized minimal disturbances on the edge of laminar–turbulent attractor have a kinetic energy density E that decreases with Reynolds number: see Hof *et al.* (2004) and Lemoult, Aider & Wesfield (2012) for experimental evidence showing a similar decreasing disturbance amplitude needed to trigger transition. No self-consistent theory has been provided for the Reynolds number scaling of such minimal disturbances. This study is partially motivated by a possible theoretical resolution to that problem using a formal asymptotic analysis and numerical evidence based on the Navier–Stokes equations.

Our idea is to use exact coherent structures as ideal specimens to examine asymptotic scaling of a particular type of coherent structure. Tracing the solution branch of the exact coherent structures at large Reynolds number, we can separate the coherent structures at various scales, which are usually entangled in a complicated transition or turbulent dynamics. Our main concern in this short paper is a self-consistent theoretical explanation of the scaling of coherent structures, rather than the numerical solutions themselves. Further computational study should be performed in the future to find more dynamically important solutions that could be combined with dynamical systems theory to relate the scaling of exact coherent structures and actual dynamics of coherent structures (see Kawahara & Kida 2001; Gibson, Halcrow & Cvitanović 2008; Willis, Cvitanović & Avila 2013). The asymptotic theory would also help to understand the qualitative structure of the high-dimensional phase space associated with large Reynolds number shear flows.

In § 2 we will construct a general asymptotic theory to connect known asymptotic theories and new small-scale states, which is the main subject of the present study. Our Navier–Stokes computational results are also shown in the same section to verify the asymptotic scaling. Then we shall discuss the implication of our results in § 3.

2. Asymptotic analysis and numerical results

We consider a shear flow governed by incompressible Navier–Stokes equations

$$(\partial_t + \boldsymbol{u}\cdot\boldsymbol{\nabla})\boldsymbol{u} = -\boldsymbol{\nabla}p + Re^{-1}\boldsymbol{\nabla}^2\boldsymbol{u}, \quad \boldsymbol{\nabla}\cdot\boldsymbol{u} = 0. \tag{2.1}$$

Here we assume that in Cartesian coordinates (x, y, z) the velocity field $\boldsymbol{u} = (u, v, w)$ and the pressure field p are periodic in x and z. For definiteness, unless otherwise noted, we restrict our attention to plane Couette flow, where $\boldsymbol{u} = (\pm 1, 0, 0)$ is satisfied at $y = \pm 1$. This means that (2.1) is non-dimensionalized by choosing the half-channel height h_*, the wall speed U_* and the fluid density ρ_* as length, velocity and density scales, respectively. There are three parameters: streamwise wavenumber α, spanwise

https://doi.org/10.1017/jfm.2015.514 Published online by Cambridge University Press

wavenumber β and Reynolds number $Re = U_* h_*/\nu$ defined by the kinematic viscosity of the fluid ν. Well established, non-trivial solutions of this system can be accurately computed by Newton's method. In this work all numerical solutions are generated by the code developed in Deguchi, Hall & Walton (2013). The spatial resolution of the solutions is carefully checked as in that paper.

Our starting point is the known steady exact coherent structures of VWI type shown in figure 1(*a*), where the wavenumber dependence of the drag on the lower wall D is plotted for various Re. This solution is the same as that discussed in Nagata (1990), Wang *et al.* (2007), Hall & Sherwin (2010), Blackburn, Hall & Sherwin (2013) and Deguchi & Hall (2014*a*,*b*). The asymptotically converged branches at relatively small β in the figure correspond to VWI. It has been shown by Blackburn *et al.* (2013) that increasing the wavenumbers causes the VWI states to begin to localize around $y = 0$. Here, we further find that when the wavenumbers become larger and reach a certain threshold size, the convergence of VWI is lost, as the deviation of the saddle-nodes at different Re in the figure suggests. The breakdown of the asymptotic convergence is in fact a signature of new asymptotic structure, which can be seen in the rescaled drag–wavenumber plot shown in figure 1(*b*), and in the self-similar flow fields at the saddle-nodes shown in figure 1(*c*). Approximately 200–300 Chebyshev polynomials are used in y to resolve the vertically localized structures. The precise definitions of the scaled wavenumber $\beta_0 \approx Re^{-1/2}\beta$ and the scaled drag $d_0 \approx Re^{1/2}\beta_0(D-1)$ used in figure 1(*b*) are to be deduced in our generalized asymptotic analysis below.

First, it is convenient to define a streamwise average operator $\overline{I}(f) = (\alpha/2\pi)\int_0^{2\pi/\alpha} f\,\mathrm{d}x$ and $\widetilde{I}(f) = f - \overline{I}(f)$ for a function $f(x, y, z)$. Using these operators, the total flow can be decomposed into the 'vortex' component $[\overline{\boldsymbol{u}}, \overline{p}] = \overline{I}([\boldsymbol{u}, p])$ and the 'wave' component $[\widetilde{\boldsymbol{u}}, \widetilde{p}] = \widetilde{I}([\boldsymbol{u}, p])$. For the vortex component we refer to $\overline{u}$ as streak and $[\overline{v}, \overline{w}]$ as roll. Then, we apply a scaling

$$[x, y, z] = [\alpha^{-1}X, \beta^{-1}Y, \beta^{-1}Z], \tag{2.2a}$$

$$[\overline{u}, \overline{v}, \overline{w}, \overline{p}] = \beta Re^{-1}[Q\gamma\overline{U}, \overline{V}, \overline{W}, \beta Re^{-1}\overline{P}], \tag{2.2b}$$

$$[\widetilde{u}, \widetilde{v}, \widetilde{w}, \widetilde{p}] = \rho\beta[\gamma\widetilde{U}, \widetilde{V}, \widetilde{W}, Q\beta Re^{-1}\widetilde{P}], \tag{2.2c}$$

where γ is the wavenumber ratio β/α, and the parameter Q is to be specified later. The size of the wave amplitude ρ is also to be fixed so that the wave drives the vortex. The scaling makes the vortex part of (2.1) fully viscous as

$$[\overline{V}\partial_Y + \overline{W}\partial_Z - \Delta]\begin{bmatrix}\overline{U}\\ \overline{V}\\ \overline{W}\end{bmatrix} + \begin{bmatrix}0\\ \partial_Y\overline{P}\\ \partial_Z\overline{P}\end{bmatrix} = -\rho^2 Re^2\overline{I}\left([\widetilde{U}\partial_X + \widetilde{V}\partial_Y + \widetilde{W}\partial_Z]\begin{bmatrix}Q^{-1}\widetilde{U}\\ \widetilde{V}\\ \widetilde{W}\end{bmatrix}\right), \tag{2.3}$$

$$\partial_Y\overline{V} + \partial_Z\overline{W} = 0, \tag{2.4}$$

while the size of the viscous term in the wave part of (2.1) is controlled by the parameter Q as

$$[\overline{U}\partial_X + Q^{-1}(\overline{V}\partial_Y + \overline{W}\partial_Z - \gamma^{-2}\partial_{XX} - \Delta)]\begin{bmatrix}\widetilde{U}\\ \widetilde{V}\\ \widetilde{W}\end{bmatrix} + [\widetilde{V}\partial_Y + \widetilde{W}\partial_Z]\begin{bmatrix}\overline{U}\\ Q^{-1}\overline{V}\\ Q^{-1}\overline{W}\end{bmatrix} + \begin{bmatrix}\gamma^{-2}\partial_X\widetilde{P}\\ \partial_Y\widetilde{P}\\ \partial_Z\widetilde{P}\end{bmatrix}$$

$$= -\rho Re Q^{-1}\widetilde{I}\left([\widetilde{U}\partial_X + \widetilde{V}\partial_Y + \widetilde{W}\partial_Z]\begin{bmatrix}\widetilde{U}\\ \widetilde{V}\\ \widetilde{W}\end{bmatrix}\right), \tag{2.5}$$

$$\partial_X\widetilde{U} + \partial_Y\widetilde{V} + \partial_Z\widetilde{W} = 0, \tag{2.6}$$

https://doi.org/10.1017/jfm.2015.514 Published online by Cambridge University Press

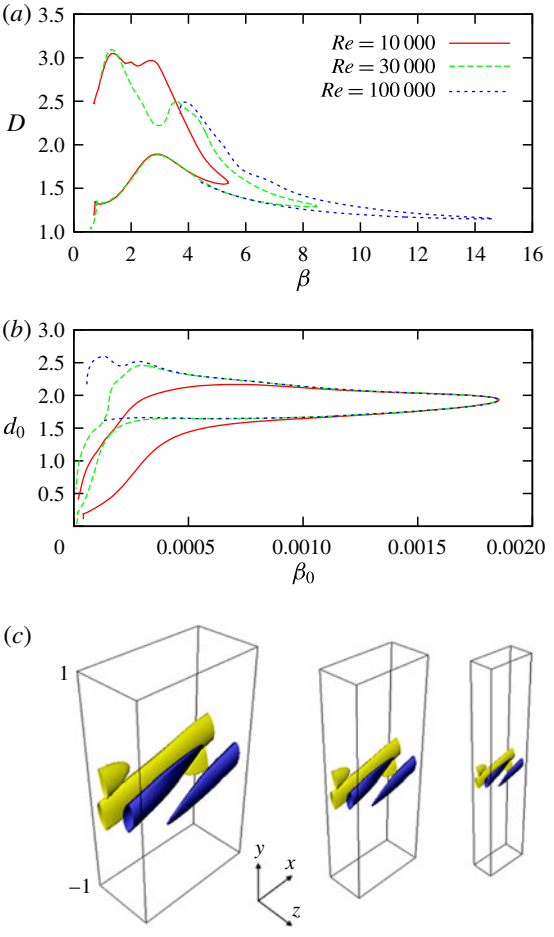


FIGURE 1. The wavenumber dependence of the steady solutions. The wavenumber ratio is fixed as $\beta/\alpha = 2$. (*a*) The variation of the drag D against the change of β. (*b*) The same result as (*a*) but both axes are rescaled. The scaled drag and wavenumber are defined as $d_0 = (\beta/D)(D-1) \approx Re^{1/2}\beta_0(D-1)$ and $\beta_0 = \sqrt{(\beta^2 - \beta d_0)/Re} \approx Re^{-1/2}\beta$, respectively. (*c*) The flow fields at the saddle-nodes. *Re* increases from left to right. The yellow and blue surfaces represent $\pm 50\,\%$ streamwise vorticity.

where $\Delta = \partial_{YY} + \partial_{ZZ}$. Here we assume steadiness of velocity fields for the sake of simplicity, but clearly the following analysis is applicable to travelling waves if we apply Galilean transformation. Notice that the periodic domain is normalized as $X \in [0, 2\pi]$ and $Z \in [0, 2\pi]$, and that no approximation has been made at this stage. As a consequence of the decomposition, we see that the vortex equations (2.3)–(2.4) must be forced by the Reynolds stress terms appearing on the right-hand side of (2.3). If these terms are not present, the vortex component must ultimately decay due to the absence of the energy input.

When $\beta \sim O(1)$, we must apply the no-slip conditions on the walls in the vertical direction. However, if β becomes asymptotically large, the conditions may be changed if we consider the nonlinear interaction is localized in a 'production layer' of thickness $O(\beta^{-1})$ where the coherent structure is produced; see figure 1(*c*). This means that we

https://doi.org/10.1017/jfm.2015.514 Published online by Cambridge University Press

assume the walls do not affect the state and the problem can be simplified to that of an infinite domain in the y direction with matching conditions to the outer flow. Hereafter, we assume all the scaled variables $[U, V, W, P, X, Y, Z]$ are $O(1)$ in the production layer, and we require that outside the layer the wave components decay for large $|Y|$, and the vortex components return to the unforced linear shear as

$$\overline{U} \to Y \mp d_0, \quad \text{as } Y \to \pm\infty, \tag{2.7}$$

where d_0 is determined as a part of a solution. Thus, from (2.2*c*) and (2.7), above and beneath the production layer, the flow must be in the form

$$\boldsymbol{u}_{\pm} = [(\gamma\beta Q/Re)(\beta y \mp d_0), 0, 0], \tag{2.8}$$

where $+$ and $-$ refer to the solutions above and beneath the production layer, respectively. These solutions of linear profile are valid solutions for whole outer regions. The gradient of the outer flow (2.8) must be equal to the drag D, and $d_0 = \beta(D-1)/D$ must be satisfied from the boundary conditions on the wall. From these conditions we have

$$D = \frac{\beta}{\beta - d_0} = \frac{\beta^2\gamma Q}{Re}. \tag{2.9}$$

The treatment of the matching to the outer flow is similar to that given in Deguchi & Hall (2014*a*).

Now, let us consider asymptotically large Re. Three distinct types of asymptotic theories can be considered depending on the size of Q and γ. The first case corresponds to VWI appearing when $Q \gg 1$; see Hall & Smith (1991), Hall & Sherwin (2010), Blackburn *et al.* (2013) and Deguchi & Hall (2014*a*,*b*). In this case (2.5) becomes inviscid apart from the critical layer occurring when $\overline{U}$ is small. As shown in Hall & Smith (1991), outside the critical layer (2.5)–(2.6) can be reduced to Rayleigh's equation for the streak, which has a singularity at the critical layer and thus produces a large-amplitude neutral wave there. Inside the critical layer of relative thickness $O(Q^{-1/3})$, the wave Reynolds stress drives the vortex component when $\rho = Re^{-1}Q^{-1/6}$. The massive reduction of the equations in the critical layer allows us to handle the structure there almost analytically, as found in Hall & Smith (1991).

As shown in figure 2(*a*), the full Navier–Stokes steady solution first appears at $Re = 127.7$ and then its existence region expands with increasing Re. In the wavenumber plane, VWI describes the behaviour of the solutions at the centre of the existence region; see the schematic picture in figure 2(*b*). The states with wavenumbers of $O(1)$ correspond to the edge of laminar–turbulent attractors discussed by Wang *et al.* (2007). In this case, since the basic flow is inviscidly stable from Rayleigh's inflection point theorem, $\overline{U}$ must have an $O(1)$ deviation from the basic flow to generate a Rayleigh wave. When the wavenumbers are increased, the solutions have a vertically localized structure, which is self-similar for fixed γ, as shown by Blackburn *et al.* (2013) and Deguchi & Hall (2014*a*); the former authors claim that the wave energy of the states satisfies Kolmogorov's 5/3 rule. There exists a critical value of $\gamma \approx 1.5$ at which the solutions cease to exist. This boundary is consistent with the minimal box size to sustain numerical turbulence reported by Hamilton *et al.* (1995).

The second case occurs when $Q, \gamma \sim O(1)$ and corresponds to the new structure seen in figure 1. This case is similar to the structure found by Deguchi & Hall (2014*c*) for boundary layer flows, where no term drops off from the Navier–Stokes equations at the limit, although here we must consider asymptotically large wavenumbers as

https://doi.org/10.1017/jfm.2015.514 Published online by Cambridge University Press

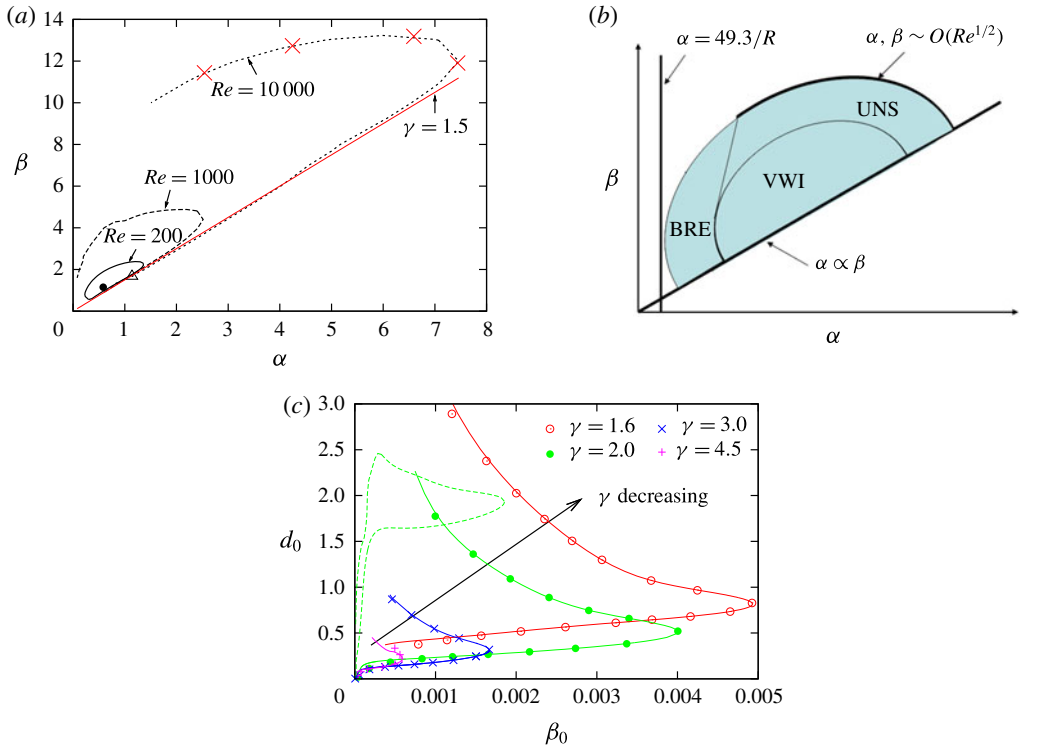


FIGURE 2. (*a*) Existence region of the steady solutions in the wavenumber plane. The circle shows $(\alpha, \beta) = (0.58, 1.15)$ where the solutions first emerge at $Re = 127.7$; see Clever & Busse (1997). The triangle is the minimal flow unit $(\alpha, \beta) = (1.14, 1.667)$ given by Hamilton, Kim & Waleffe (1995). The crosses correspond to the saddle-nodes shown in (*c*). (*b*) A schematic picture of the existence region inferred from our generalized asymptotic analysis. (*c*) Bifurcation diagram of the steady solutions for various $\beta/\alpha = \gamma$. The curves are for $Re = 30\,000$, while the points are for $Re = 10\,000$. The saddle-nodes of asymptotically converged solutions shown by the solid curves define the crosses in (*a*). The dashed curve shows the branch seen in figure 1(*a*) for $Re = 30\,000$.

we have seen in figure 1. In fact, it is easy to confirm that in the production layer (2.1) can be rescaled into unit Reynolds number Navier–Stokes equations (UNS) by using the velocity scale $[u] \sim Re^{-1/2}$ and the length scale $[x] \sim Re^{-1/2}$ for all three components. The scaling can be found from (2.2*a*)–(2.2*c*) together with the fact that ρ must be $O(Re^{-1})$ to drive the vortex, or alternatively from the viscous–convective balance $[u][x] \sim Re^{-1}$ and $[u] \sim [x]$ from (2.7). The wavenumber must be expanded as $\beta = \beta_0 Re^{1/2} + \cdots$ and this means that it is appropriate to define $\beta_0 = 1/\sqrt{\gamma Q}$ so that β satisfies

$$\beta^2 - \beta d_0 - \beta_0^2 Re = 0, \tag{2.10}$$

using (2.9). From (2.9)–(2.10), d_0 and β_0 can be computed from D, β and Re to confirm the asymptotic convergence of UNS states as seen in figure 1(*b*). The fact that no reduction is possible in the production layer implies that the analysis there must rely on computations as opposed to the semi-analytic critical layer analysis. In fact, production layer solutions are most easily obtained by applying the knowledge of the asymptotic theory to the Navier–Stokes computations for high Reynolds

https://doi.org/10.1017/jfm.2015.514 Published online by Cambridge University Press

number. In the wavenumber plane, UNS states describe the large-wavenumber boundary of the existence region as shown in figure 2(*b*). The crosses indicated at the numerically obtained boundary in figure 2(*a*) correspond to the asymptotically converged saddle-nodes shown by solid curves in figure 2(*c*). In the continuation process of the solution branch in the parameter space, it is found that the branch behaves in a complicated way and several families of saddle-nodes appear. The family of saddle-nodes corresponding to the solid curve in figure 2(*c*) is found to be different from that seen in figure 1 (the same result is shown by a dashed curve in figure 2*c*). We can connect these solution branches by changing wavenumbers.

In the third case, $Q \sim O(1)$ and $\gamma \gg 1$, and (2.1) reduces to boundary region equations (BRE), i.e. the streamwise derivative is neglected in the pressure and viscous terms in the Navier–Stokes equations; see Deguchi *et al.* (2013). We can prove that there is no BRE-type solution for streamwise wavenumber smaller than some particular threshold. As shown in Deguchi *et al.* (2013), that threshold is given by $\alpha = 49.3/Re$ for plane Couette flow; see figure 2(*a*). However, notice that numerical evidence has shown that some solutions developing multiple spatial scales in x could exist beyond that threshold because it is only applicable for purely BRE-type solutions; see Avila *et al.* (2013), Brand & Gibson (2014), Deguchi & Hall (2014*b*) and Zammert & Eckhardt (2014) for numerical evidence of the multiple-scale solutions. The longest streamwise wavelength structure, where the BRE-type problem predicts $\alpha \sim O(Re^{-1})$, carries a largest $O(1)$ disturbance, and thus may be related to the energetic very large-scale motion observed in Morrison *et al.* (2004).

3. Discussion and conclusions

Importantly, the UNS-type exact coherent structures found in this study are fully viscous and thus must have a Kolmogorov length/velocity scale. In fact, by using a dimensional energy dissipation rate $\Phi = \nu(U_*/h_*)^2$, we can find the Kolmogorov length scale $\sim(\nu^3/\Phi)^{1/4} = Re^{-1/2}h_*$ and Kolmogorov velocity scale $\sim(\nu\Phi)^{1/4} = Re^{-1/2}U_*$ consistent with the discussion in the last section. Although the solutions of this type have a very small disturbance size, some of them can trigger a transition to turbulence. Figure 3 shows the typical direct numerical simulations starting from the UNS- and VWI-type solutions perturbed by a small random disturbance. Both solutions sit at the laminar–turbulent boundaries, but UNS-type solutions have much smaller disturbance kinetic energy E, averaged in the periodic box. Note that, in an asymptotic sense, any disturbance of smaller size must dissipate since only the viscous terms play a major role. Therefore UNS states represent the theoretically minimal self-sustained states. Another implication of our theory is that no reduced model can be considered for such minimal-scale coherent structures, since we need to keep all terms in the Navier–Stokes equations.

In view of much numerical evidence for the existence of the multiple-scale solutions localized in (x, z), for example Brand & Gibson (2014) and Zammert & Eckhardt (2014), a localized version of our minimal scale states may also exist. It is noteworthy that such localized minimal states would have an energy scaling $E \sim Re^{-2.5}$ in a fixed periodic box, which is close to that obtained by an energy-optimized technique, $E \sim Re^{-2.7}$; in fact, the optimized states typically have localized structures as seen in Duguet *et al.* (2013).

Although our focus so far has been on steady solutions, the scenario elucidated here can be applicable for any form of UNS solutions, such as travelling-wave, time-periodic or even chaotic solutions, by introducing a time scale $\sim[x]/[u]$.

https://doi.org/10.1017/jfm.2015.514 Published online by Cambridge University Press

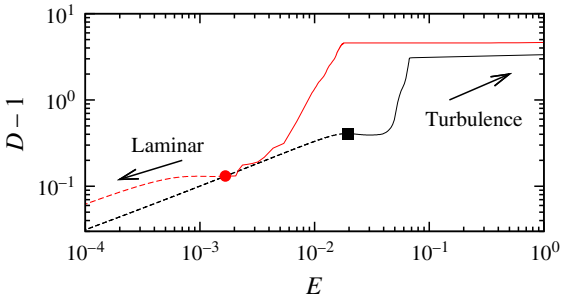


FIGURE 3. The direct numerical simulation for $Re = 10\,000$. A periodic box $(x, y, z) \in [0, 2\pi/1.5] \times [-1, 1] \times [0, 2\pi/3]$ is resolved by $145 \times 410 \times 98$ grid points. The circle is the UNS-type solution for $(\alpha, \beta) = (6, 12)$; this solution is close to the saddle-node of the solid curve for $\gamma = 2$ in figure 2(*c*). The square is the VWI-type solution for $(\alpha, \beta) = (1.5, 3)$ at the lower branch of figure 1(*a*). The solutions are perturbed by random disturbances with $E \sim O(10^{-16})$, and the two typical results are shown for each solution. Note that for the laminar flow $(D, E) = (1, 0)$. The turbulent trajectory is not shown since the resolution used is insufficient to produce correct turbulent statistics.

Furthermore, similar to the localized VWI proposed by Blackburn *et al.* (2013), the UNS results found in plane Couette flow can be embedded for any background flow as long as the flow can be locally approximated by a linear shear in the asymptotic sense. When that local approximation is not applicable, we need to consider different far-field boundary conditions for UNS. For example, at a point where the background shear vanishes, a local approximation of the background flow may be proportional to the square of the vertical coordinate after an appropriate Galilean transformation. Thus the far-field condition (2.7) must be replaced by $\overline{U} \to Y^2$ to leading order. Such a UNS problem can be solved at the centre of the plane Poiseuille flow, where the basic flow takes the form of $\boldsymbol{u} = [1 - y^2, 0, 0]$. Figure 4 shows an example of such UNS-type solutions. Notice that in general the UNS states must travel with a local basic flow speed plus a correction of order $[u]$. The appropriate wavenumber scaling $\sim[x]^{-1}$ can easily be found by considering the viscous–convective balance $[u][x] \sim Re^{-1}$ and the far-field condition $[u] \sim [x]^2$. The scaling $[u] \sim Re^{-2/3}$, $[x] \sim Re^{-1/3}$ can be confirmed in figure 4(*a*), where the scaled wave speed and wavenumber are plotted. Likewise at the edge of boundary layers, the form of the background flow is typically of exponential function form, and in fact this case corresponds to the free-stream coherent structures observed at the edge of boundary layers; see Deguchi & Hall (2014*c*). However, notice that the states discussed here are completely trapped in the production layer whilst the free-stream coherent structures generate a large streak beneath the production layer.

The UNS-type structures may also be found in the near-wall region of turbulent shear flows, where small-scale coherent structures play a major role. When the UNS structure is close to the wall we must apply no-slip conditions at finite Y instead of one of the far-field conditions. The near-wall fine-scale exact coherent structures found by Gibson & Brand (2014) are likely to have a UNS limit of this kind.

In conclusion, we have found an asymptotic theory for large Reynolds number that describes self-sustained nonlinear coherent structures at Kolmogorov microscale. The self-sustaining mechanism of the structure is governed by unit Reynolds number Navier–Stokes equations in an unbounded domain. Solutions of that canonical

https://doi.org/10.1017/jfm.2015.514 Published online by Cambridge University Press

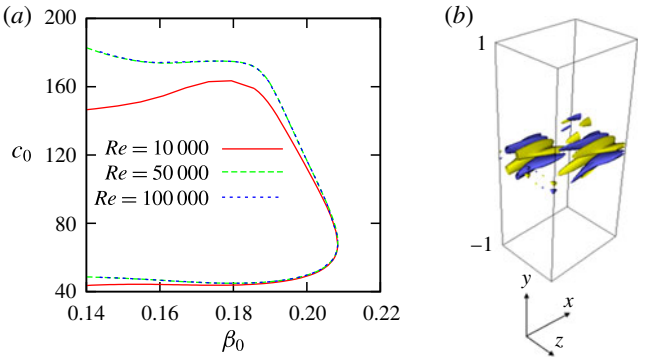


FIGURE 4. (*a*) The bifurcation diagram of the plane Poiseuille flow solutions for $\gamma = 4/3$. The solutions are obtained from TW1-1 found in Gibson & Brand (2014) and thus are of the travelling-wave form propagating in x with a phase speed c. To show the solutions are of UNS type, $c_0 = (1 - c)Re^{2/3}$ and $\beta_0 = Re^{-1/3}\beta$ are used in the diagram. (*b*) The flow field at the saddle-node for $Re = 100\,000$. See the caption to figure 1 for the definition of the surfaces.

problem can be found by directly solving simple parallel flows at large Reynolds number. The asymptotic solutions obtained in this way define the theoretically minimal-scale self-sustained structures that can be embedded at a local position of almost arbitrary shear flows. Our numerical computation suggests that some disturbances at Kolmogorov scale can initiate a turbulent transition despite their finite but asymptotically small size. Therefore, our results seems to be an important stepping stone to elucidating the puzzling property of shear flows noticed by Sommerfeld (1908). Notice that the conclusion drawn here does not contradict the belief that some numerically obtained optimal disturbances are on the stable manifold of the edge state of VWI/self-sustaining process type, as the UNS-type equilibrium states could have a heteroclinic connection to the edge state.

Acknowledgements

Discussions with Professors M. Nagata and P. Hall, and the useful comments made by the anonymous referees are gratefully acknowledged.

References

AVILA, M., MELLIBOVSKY, F., ROLAND, N. & HOF, B. 2013 Streamwise-localized solutions at the onset of turbulence in pipe flow. *Phys. Rev. Lett* **110**, 224502.

BLACKBURN, H. M., HALL, P. & SHERWIN, S. 2013 Lower branch equilibria in Couette flow: the emergence of canonical stats for arbitrary shear flows. *J. Fluid Mech.* **726**, R2.

BRAND, E. & GIBSON, J. F. 2014 A doubly localized equilibrium solution of plane Couette flow. *J. Fluid Mech.* **750**, R3.

CLEVER, R. M. & BUSSE, F. H. 1997 Tertiary and quaternary solutions for plane Couette flow. *J. Fluid Mech.* **344**, 137–153.

DEGUCHI, K. & HALL, P. 2014*a* Canonical exact coherent structures embedded in high Reynolds number flows. *Phil. Trans. R. Soc. Lond.* A **372**, 20130352, 1–19.

DEGUCHI, K. & HALL, P. 2014*b* The high Reynolds number asymptotic development of nonlinear equilibrium states in plane Couette flow. *J. Fluid Mech.* **750**, 99–112.

https://doi.org/10.1017/jfm.2015.514 Published online by Cambridge University Press

DEGUCHI, K. & HALL, P. 2014*c* Free-stream coherent structures in parallel boundary-layer flows. *J. Fluid Mech.* **752**, 602–625.

DEGUCHI, K., HALL, P. & WALTON, A. G. 2013 The emergence of localized vortex–wave interaction states in plane Couette flow. *J. Fluid Mech.* **721**, 58–85.

DUGUET, Y., MONOKROUSOS, A., BRANDT, L. & HENNINGSON, D. 2013 Minimal transition thresholds in plane Couette flow. *Phys. Fluids* **25**, 084103.

GIBSON, J. F. & BRAND, E. 2014 Spanwise-localized solutions of planar shear flows. *J. Fluid Mech.* **745**, 25–61.

GIBSON, J. F., HALCROW, J. & CVITANOVIĆ, E. 2008 Visualizing the geometry of state space in plane Couette flow. *J. Fluid Mech.* **611**, 107–130.

HALL, P. & SHERWIN, S. 2010 Streamwise vortices in shear flows: harbingers of transition and the skeleton of coherent structures. *J. Fluid Mech.* **661**, 178–205.

HALL, P. & SMITH, F. T. 1991 On strongly nonlinear vortex/wave interactions in boundary-layer transition. *J. Fluid Mech.* **227**, 641–666.

HAMILTON, J. M., KIM, J. & WALEFFE, F. 1995 Regeneration mechanisms of near-wall turbulence structures. *J. Fluid Mech.* **287**, 317–348.

HOF, B., VAN DOORNE, C. W. H., WESTERWEEL, J., NIEUWSTADT, F. T. M., FAISST, H., ECKHARDT, B., WEDIN, H., KERSWELL, R. R. & WALEFFE, F. 2004 Experimental observation of nonlinear traveling waves in turbulent pipe flow. *Science* **305** (5690), 1594–1598.

ITANO, T. & TOH, S. 2001 The dynamics of bursting process in wall turbulence. *J. Phys. Soc. Japan* **70**, 703–716.

KAWAHARA, G. & KIDA, S. 2001 Periodic motion embedded in plane Couette turbulence: regeneration cycle and burst. *J. Fluid Mech.* **449**, 291–300.

LEMOULT, G., AIDER, J.-L. & WESFIELD, J. E. 2012 Experimental scaling law for the subcritical transition to turbulence in plane Poiseuille flow. *Phys. Rev.* E **85**, 025303.

MORRISON, J. F., MCKEON, B. J., JIANG, W. & SMITS, A. J. 2004 Scaling of the streamwise velocity component in turbulent pipe flow. *J. Fluid Mech.* **508**, 99–131.

NAGATA, M. 1990 Three-dimensional finite-amplitude solutions in plane Couette flow: bifurcation from infinity. *J. Fluid Mech.* **217**, 519–527.

NISHIOKA, M., IIDA, S. & ICHIKAWA, Y. 1975 An experimental investigation of the stability of plane Poiseuille flow. *J. Fluid Mech.* **72**, 731–751.

SOMMERFELD, A. 1908 Ein Beitrag zur hydrodynamischen Erlärung der turbulenten Flüssigkeitsbewegungen. *Atti del 4. Congr. Internat. Math. Roma* **3**, 116–124.

WANG, J., GIBSON, J. F. & WALEFFE, F. 2007 Lower branch coherent states: transition and control. *Phys. Rev. Lett.* **98**, 204501.

WALEFFE, F. 1997 On a self-sustaining process in shear flows. *Phys. Fluids* **9**, 883–900.

WALEFFE, F. 2003 Homotopy of exact coherent structures in plane shear flows. *Phys. Fluids* **15**, 1517–1534.

WILLIS, A. P., CVITANOVIĆ, P. & AVILA, M. 2013 Revealing the state space of turbulent pipe flow by symmetry reduction. *J. Fluid Mech.* **721**, 514–540.

ZAMMERT, S. & ECKHARDT, B. 2014 Streamwise and doubly-localised periodic orbits in plane Couette flow. *J. Fluid Mech.* **761**, 348–359.

https://doi.org/10.1017/jfm.2015.514 Published online by Cambridge University Press